Ultra-broadband mode multiplexers based on three-dimensional asymmetric waveguide branches

Wu, Yunfei; Chiang, Kin Seng

Published in:
Optics Letters

Published: 01/02/2017

Document Version:
Post-print, also known as Accepted Author Manuscript, Peer-reviewed or Author Final version

Published version (DOI):
10.1364/OL.42.000407

Publication details:
Wu, Y., & Chiang, K. S. (2017). Ultra-broadband mode multiplexers based on three-dimensional asymmetric waveguide branches. *Optics Letters*, *42*(3), 407-410. https://doi.org/10.1364/OL.42.000407

Ultra-broadband mode multiplexers based on three-dimensional asymmetric waveguide branches

YUNFEI WU AND KIN SENG CHIANG*

Department of Electronic Engineering, City University of Hong Kong, 83 Tat Chee Avenue, Kowloon, Hong Kong SAR, China
**Corresponding author: eeksc@cityu.edu.hk*

Received XX Month XXXX; revised XX Month, XXXX; accepted XX Month XXXX; posted XX Month XXXX (Doc. ID XXXXX); published XX Month XXXX

We propose a three-dimensional waveguide mode multiplexer structure that operates on the principle of adiabatic mode transition along multilayer asymmetric waveguide branches. Using this structure, we designed and fabricated a three-mode and a four-mode multiplexer with polymer material, which can operate over the C+L band and beyond with small modal crosstalk (< −10 dB) and negligible polarization dependence, and be directly connected to fibers with low loss. They could be used as mode-selective devices for ultra-broadband mode-division multiplexing based on few-mode fibers.

OCIS codes: (130.3120) Integrated optics devices; (130.5460) Polymer waveguides; (060.1810) Buffers, couplers, routers, switches, and multiplexers; (060.2330) Fiber optics communications.

http://dx.doi.org/10.1364/OL

Mode-division multiplexing (MDM), which exploits the spatial dimension of single-core or multi-core few-mode fibers (FMFs) to increase the fiber transmission capacity, has attracted much interest in recent years [1–3]. A critical device in an MDM system is a mode multiplexer, which serves to spatially combine or separate the individual spatial modes [4,5] or mode groups [6] of an FMF. Mode multiplexers are also required for the compensation of mode-dependent losses and delays in MDM systems [7]. In this paper, we propose and demonstrate ultra-broadband mode multiplexers with high spatial-mode selectivity.

Compact mode multiplexers with high spatial-mode selectivity can be realized with various physical mechanisms, such as mode-pattern construction with multi-plane light conversion [8], resonant mode coupling with directional couplers [9–13], and adiabatic mode transition with structures like tapered directional couplers [14,15], asymmetric Y branches [16,17], and photonic lanterns [18]. Fiber-based multiplexers [13,18] allow direct splicing with fibers, but require specially prepared fibers and difficultly controlled fabrication processes. On the other hand, waveguide-based multiplexers can be fabricated with the micro-fabrication technology based on photolithography, which is more flexible and controllable and also allows for device integration. However, common planar waveguide platforms have difficulty in multiplexing high-order fiber modes whose fields oscillate in the vertical direction. The problem can be solved by inserting specially designed mode rotators in a planar mode multiplexer [12], which, however, adds much complication to the device layout. A natural way to multiplex fiber modes is to employ three-dimensional (3D) waveguide structures, such as a structure that combines horizontal and vertical directional couplers [9–11,14,15]. Such 3D waveguide multiplexers can be fabricated relatively easily with polymer by spin-coating and photolithography [10,11,15], or with boro-aluminosilicate glass by direct laser writing [9,14].

Among the various mode-multiplexing mechanisms, adiabatic mode transition along asymmetric waveguide branches has the merits of ultra-broadband operation and relaxed fabrication tolerance. The waveguide branches experimentally demonstrated so far for mode multiplexing are planar structures [16,17], which have limited capacity for processing high-order fiber modes, as mentioned earlier. In this paper, we propose a 3D mode multiplexer structure where a segmented few-mode core is branched out into a number of dissimilar single-mode cores in multiple layers, which can be considered as a stack of interacting 3D asymmetric Y branches. Using this structure, we designed and fabricated a three-mode and a four-mode multiplexer with polymer, which can operate over the C+L band and beyond with crosstalk smaller than −10 dB and negligible polarization dependence, and be directly connected to optical fibers with low loss. Compared with previously reported mode multiplexers, our devices offer a much wider bandwidth, which is important for the development of ultra-broadband MDM systems, where each spatial mode or mode group is expected to carry independent dense wavelength-division-multiplexed channels.

Fig. 1(a) shows the structure of the proposed three-mode multiplexer. The device has a single rectangular few-mode core with width W and height H at one end (the multiplexing end), partition ratios a and b. The three segments branch out gradually into three dissimilar single-mode cores at the other end (the demultiplexing end). The core in the upper layer (Core 1) follows a straight path and is tapered down into half of its original width to ensure single-mode operation at the de-multiplexing end. The two cores in the lower layer (Core 2 and Core 3) form a planar asymmetric Y branch with two cosine S-bends. The few-mode core

at the multiplexing end supports the E_{11}, E_{21}, and E_{12} modes, which match well with the LP_{01}, LP_{11a}, and LP_{11b} fiber modes, respectively. Over a device length L, the three cores are spatially separated by a distance D.

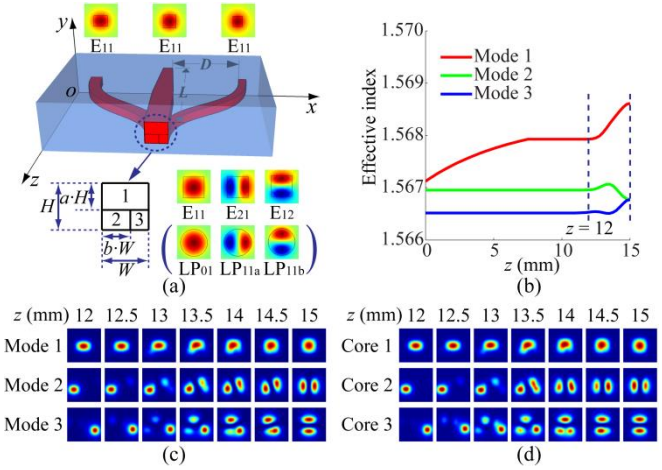

Fig. 1. (a) Structure of the proposed three-mode multiplexer; (b) simulated effective indices and (c) intensity distributions of the local modes along the device and (d) simulated evolutions of intensity patterns along the device from z = 12 to 15 mm with the fundamental modes launched into Core 1, Core 2, and Core 3, respectively. The results are obtained for the x polarization at the wavelength 1550 nm with W = 12 μm, H = 12 μm, a = 0.575, b = 0.6, D = 127 μm, L = 15 mm, a core index of 1.570, and a cladding index of 1.566.

The mode multiplexer operates on the principle of adiabatic mode transition, where the E_{11}, E_{21}, and E_{12} modes of the few-mode core evolve into the E_{11} modes of Core 1, Core 2, and Core 3, respectively. By allowing a single rectangular few-mode core to branch out into three cores in two layers, spatial modes with symmetric and anti-symmetric field distributions in both the horizontal and vertical directions can be (de)multiplexed, which is difficult to achieve with conventional planar waveguide structures. To facilitate adiabatic mode transition, the three cores should be sufficiently dissimilar to avoid degeneracy among the local modes, i.e., the effective indices of the three cores should be sufficiently different to avoid phase-matching and hence significant power exchange among them. Therefore, full multiplexing of the three modes cannot be achieved with b = 0.5, for which Core 2 and Core 3 are identical. To limit the loss caused by the 3D waveguide branches and the fiber-coupling losses, the three cores should not be too small, i.e., b should not be close to 0 or 1. The partition ratios a and b should be properly chosen for the achievement of low-crosstalk performance.

We first illustrate the operation of the device with numerical simulation. As a typical example, we take W = 12 μm, H = 12 μm (a square few-mode core), a = 0.575, b = 0.6, D = 127 μm, and L = 15 mm. The average branching angle between the two farthest separated branches (Core 2 and Core 3) is 0.97°. The refractive indices of the core and the cladding are 1.570 and 1.566, respectively. Fig. 1(b) and Fig. 1(c) show the effective indices and the intensity distributions of the local modes for the x polarization at the wavelength 1550 nm, which are calculated with the full-vector finite-element method (COMSOL). The three local modes, Mode 1, Mode 2, and Mode 3, are non-degenerate along the device, except at the multiplexing end (z = 15 mm), where Mode 2 (E_{21}) and Mode 3 (E_{12}) are degenerate. As shown in Fig. 1(c), the three modes at z = 12 mm have different spot sizes, which follow the ranking of their effective indices shown in Fig. 1(b). Keeping the local modes non-degenerate helps to suppress couplings among these modes. To break the degeneracy of the local modes sufficiently, we may use a rectangular few-mode core with a sufficiently large aspect ratio [11]. Fig. 1(d) shows the evolutions of the intensity patterns along the device from z = 12 to 15 mm (the region marked by the two vertical dashed lines in Fig. 1(b)) for the x polarization at 1550 nm, calculated with the semi-vector beam-propagation method (RSOFT BeamPROP), where the x-polarized E_{11} modes are launched into the three single-mode cores individually. A comparison of Fig. 1(c) and Fig. 1(d) shows close agreement between the local-mode results and the beam-propagation results and thus confirms effective adiabatic mode transition. We repeat the calculation for the y polarization and obtain almost the same results. The polarization-insensitive operation of the device is due to the use of a small core-cladding refractive-index contrast.

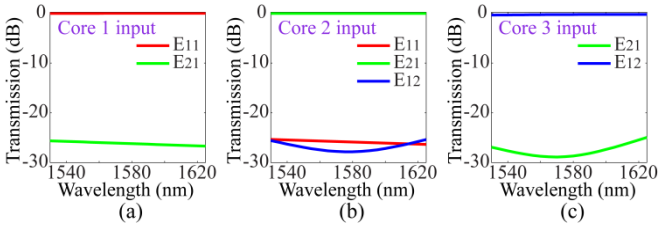

Fig. 2. Simulated transmission spectra of the E_{11}, E_{21}, and E_{12} modes in the few-mode core for the three-mode multiplexer in Fig. 1, when the x-polarized E_{11} modes of (a) Core 1, (b) Core 2, and (c) Core 3 are excited, respectively.

Fig. 2 shows the simulated transmission spectra of the E_{11}, E_{21}, and E_{12} modes in the few-mode core over the C+L band (1530 – 1625 nm), when the x-polarized E_{11} modes of Core 1, Core 2, and Core 3 are excited, respectively, where material loss and dispersion are ignored. The E_{12} mode from the few-mode core for the Core 1 input and the E_{11} mode from the few-mode core for the Core 3 input are both below –30 dB over the C+L band and, therefore, not shown in Fig. 2. As shown in Fig. 2, the E_{11}, E_{21}, and E_{12} modes of the few-mode core are selectively evolved from the E_{11} modes launched into Core 1, Core 2, and Core 3, respectively. Over the C+L band, the modal crosstalks are smaller than –25 dB. In fact, the device can operate over an even broader range of wavelengths, which is only limited by the cutoff wavelengths of the modes of the few-mode core. The very low propagation losses for Core 1, Core 2, and Core 3 over the C+L band, which are 0.01, 0.03, and 0.36 dB, respectively, confirm highly effective adiabatic mode transition. The results for the y polarization are almost identical.

We fabricated the designed device with the UV-curable polymer materials EpoCore and EpoClad (Micro Resist Technology) by the standard microfabrication process, which involves spin-coating and photolithographic patterning of polymer films layer by layer on a silicon substrate [11]. We used EpoCore as the core material and a mix of EpoCore and EpoClad (3:2 mass ratio) as the cladding material to achieve a core-cladding index contrast close to that of the commercial step-index two-mode fiber (OFS). The refractive indices of the core and the cladding material, measured on thin

films with a prism coupler (Metricon 2010) at 1536 nm, were 1.5712 (1.5704) and 1.5665 (1.5669), respectively, for the TE (TM) polarizations. The birefringence was lower than 0.001. Microscopic images of three typical fabricated devices (cleaved with a diamond pen), whose partition ratios are b = 0.5, 0.6, and 0.7, respectively, are shown in Fig. 3(a). These devices were fabricated on the same substrate to the same length and height, so they differed mainly in the partition ratio b and hence the widths of Core 2 and Core 3. The dimensions of the cores in these devices are also shown in Fig. 3(a), which are close to the values used in our design example. The total length of each device was 20 mm, which included 5 mm of straight waveguide leads at the two ends.

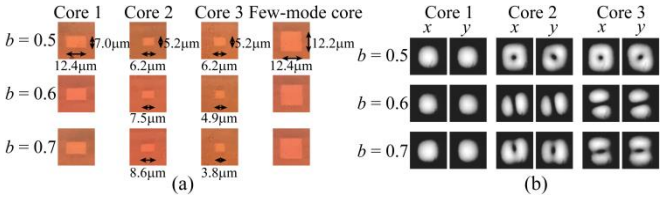

Fig. 3. (a) Microscopic images of the cores in three typical fabricated devices that have different partition ratios (b = 0.5, 0.6, and 0.7) and (b) near-field patterns obtained from the few-mode core for the x and y polarizations by launching (C+L)-band ASE light into Core 1, Core 2, and Core 3, respectively, for the three devices.

To demonstrate the operation of the device, we launched broadband light into Core 1, Core 2, and Core 3 individually with a (C+L)-band ASE source (Amonics ALS-CL-15-B-FA) and measured the corresponding near-field patterns at the few-mode ends of the devices with an infrared camera (Hamamatsu Photonics C2741-03) through a 40 x lens and a polarizer. The results are shown in Fig. 3(b). The patterns showed little difference between the x and y polarizations, which confirms polarization-insensitive operation. The device with b = 0.5 shows similar doughnut-shaped output patterns for light launched into Core 2 or Core 3, which indicates an equal mix of the E_{21} and E_{12} modes. Therefore, the device with b = 0.5 cannot (de)multiplex the E_{21} and E_{12} modes; it can (de)multiplex, however, the E_{11} mode and the E_{12}/E_{21} mode group. The other two devices can (de)multiplex all the three modes. The one with b = 0.6 show particularly clear mode patterns at its few-mode end, which suggests high mode selectivity over the entire C+L band.

Table I. Crosstalks of the three-mode multiplexer with b = 0.6 measured at 1550 nm with individual modes launched into the few-mode core.

Input fiber mode	Crosstalk (dB)		
	Core 1	Core 2	Core 3
LP_{01}	—	–20.3	–24.9
LP_{11a}	–20.0	—	–18.9
LP_{11b}	–20.6	–18.0	—

To provide an estimate of the crosstalk performance of the device, we selectively excited the modes of the few-mode core and measured the output powers from the three single-mode cores. Any power from the single-mode core that does not correspond to the intended input mode is considered to be crosstalk to that core. To selectively excite the E_{21} or E_{12} mode of the few-mode core, we used a fiber LP_{01}-LP_{11} mode converter with a mode extinction ratio of 22.9 dB at 1550 nm, which was a CO_2-laser written long-period fiber grating in a step-index two-mode fiber (OFS) [19]. This mode converter allowed the generation of clean LP_{11a} and LP_{11b} mode patterns by control of the polarization state of the input LP_{01} mode [19]. Table I lists the crosstalks measured for the device with b = 0.6 at 1550 nm, which vary from –18.0 to –24.9 dB, depending on the input mode and the output core. These crosstalks include the effects caused by the mismatch between the fiber and waveguide modes and any alignment errors. In all the measurements conducted in the present study, we applied an index-matching liquid with a refractive index of 1.5671 at 1550 nm to the fiber-waveguide interface to minimize Fresnel reflection.

We measured the fiber-waveguide coupling loss of the device with b = 0.6 by comparing the output powers measured with a short fiber lead coupled to and removed from a particular waveguide core. To measure the coupling loss of a specific mode at the few-mode end, the mode was excited by launching light into the corresponding single-mode core at the other end. The coupling losses of Core 1, Core 2, and Core 3 for a standard single-mode fiber were 0.3, 0.3, and 0.4 dB, respectively, while the coupling losses of the LP_{01}, LP_{11a}, and LP_{11b} modes for the OFS step-index two-mode fiber were 0.1, 0.3, and 0.4 dB, respectively. The insertion losses of the device (excluding the fiber-waveguide coupling losses), measured by coupling 1550-nm laser light into individual single-mode cores and detecting the power from the few-mode core, were 8.2, 8.8, and 9.3 dB for the LP_{01}, LP_{11a}, and LP_{11b} modes, respectively, which were due to material absorption and any scattering loss caused by waveguide imperfections. The mode-dependent loss variation with all the fiber-waveguide coupling losses taken into account was within ±0.8 dB. The insertion losses may be further reduced by using polymer material with lower loss and improving the waveguide fabrication process.

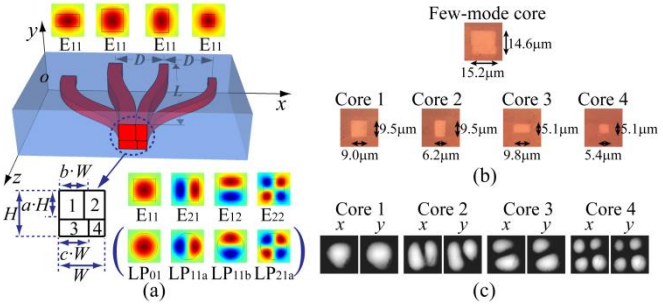

Fig. 4. (a) Structure of the proposed four-mode multiplexer; (b) microscopic images of the cores in a typical fabricated device; and (c) near-field patterns obtained from the few-mode core for the x and y polarizations by launching (C+L)-band ASE light into Core 1, Core 2, Core 3, and Core 4 of the device, respectively.

To demonstrate the scalability of the proposed 3D waveguide structure, we next present a four-mode multiplexer. Fig. 4(a) shows the structure of the multiplexer, where a few-mode core with width W and height H is divided into four segments in two layers at one end with three partition ratios a, b, and c and the four segments branch out gradually into four single-mode cores at the other end (Core 1, Core 2, Core 3, and Core 4). The few-mode core supports the E_{11}, E_{21}, E_{12}, and E_{22} modes (or the LP_{01}, LP_{11a}, LP_{11b}, and LP_{21a} fiber modes), which evolve into the E_{11} modes of Core 1,

Core 2, Core 3, and Core 4, respectively. As in the design of the three-mode multiplexer, we should properly choose the values of *a*, *b*, and *c* to provide four sufficiently dissimilar single-mode cores, so that the crosstalks among the local modes along the waveguide branches are minimized. As an example, using the same core and cladding refractive indices as for the three-mode multiplexer, we take W = 15 μm, H = 15 μm, a = 0.65, b = 0.6, c = 0.65, D = 62.5 μm, and L = 20 mm. The average branching angle between the two farthest separated branches (Core 3 and Core 4) is 0.54°. The calculated crosstalks among the four spatial modes of the few-mode core are smaller than –17 dB over the C+L band.

We fabricated the designed device with the same core and cladding polymer materials by the same process as for the three-mode multiplexer. Fig. 4(b) shows the microscopic images of a typical fabricated device together with its core dimensions, which are close to the values used in our design example. The total length of the device was 25 mm, which included 5 mm of straight waveguide leads at the two ends. Fig. 4(c) shows the near-field patterns obtained from the few-mode core for the *x* and *y* polarizations by launching the E_{11} modes into the single-mode cores individually. As shown in Fig. 4(c), the four spatial modes are clearly multiplexed with little polarization dependence.

Table II. Crosstalks of the four-mode multiplexer measured at 1550 nm with individual modes launched into the few-mode core.

Input fiber mode	Crosstalk (dB)			
	Core 1	Core 2	Core 3	Core 4
LP_{01}	—	–14.4	–21.3	–23.5
LP_{11a}	–14.5	—	–15.6	–22.5
LP_{11b}	–13.1	–11.6	—	–22.2

We measured the crosstalk performance of the four-mode multiplexer at 1550 nm in the same way as we did for the three-mode multiplexer. As we could not excite the E_{22} mode of the few-mode core with a high extinction ratio (due to the lack of an effective LP_{01}-LP_{21} mode converter), we could not measure the crosstalks with the LP_{21a} mode as the input mode. Table II lists the measured crosstalks with the other fiber modes as the input modes, which vary from –11.6 dB to –23.5 dB, depending on the input mode and the output core. Although we could not directly measure the crosstalks with the LP_{21a} mode as the input mode, our simulation results show that the crosstalks from the LP_{21a} input mode to Core 1, Core 2, and Core 3 are comparable to the crosstalks from the LP_{01}, LP_{11a}, and LP_{11b} input modes to Core 4, respectively, which, according to Table II, suggests that the crosstalks with the LP_{21a} mode as the input mode should be smaller than about –20 dB.

We also measured the coupling losses of Core 1, Core 2, Core 3, and Core 4 for a standard single-mode fiber and the results were 0.3, 0.3, 0.4, and 0.4 dB, respectively. The coupling losses of the LP_{01}, LP_{11a}, LP_{11b}, and LP_{21a} modes for the OFS step-index four-mode fiber were 0.2, 0.3, 0.5, and 0.6 dB, respectively. The insertion losses (excluding the fiber-waveguide coupling losses), measured at 1550 nm, were 8.8, 9.0, 9.6, and 9.9 dB for the LP_{01}, LP_{11a}, LP_{11b}, and LP_{21a} modes, respectively. The mode-dependent loss variation with all the fiber-waveguide coupling losses taken into account was within ±0.8 dB.

According to our simulation, for a crosstalk smaller than –10 dB at 1550 nm, the horizontal offset between the two waveguide layers should be within ±0.7 μm and ±0.8 μm for the three-mode and the four-mode multiplexer, respectively, which are within the fabrication tolerance (±0.5 μm) determined by the vernier marks on the photomask.

In conclusion, we propose a 3D waveguide mode multiplexer structure that operates on the principle of adiabatic mode transition along multilayer asymmetric Y branches. Using two-layer waveguide branches, we designed and fabricated a three-mode and a four-mode multiplexer with polymer material, which show excellent spatial-mode selectivity and low fiber-coupling losses and can operate over the C+L band and beyond with negligible polarization dependence. The proposed 3D structure can be scaled up by adding more core layers and more core segments in each layer, though a precise alignment of waveguide structures over many layers can be a serious practical challenge. Mode multiplexers built upon this 3D waveguide platform are suitable for ultra-broadband fiber-based MDM applications.

Funding. National Natural Science Foundation of China (NSFC), China (61377057)

Acknowledgment. The authors thank Dr. Wei Jin and Dr. Jiangli Dong for their technical assistance.

References

1. D. J. Richardson, J. M. Fini, and L. E. Nelson, Nat. Photonics **7**, 354 (2013).
2. G. Li, N. Bai, N. Zhao, and C. Xia, Adv. Opt. Photonics **6**, 413 (2014).
3. T. Mizuno, H. Takara, A. Sano, and Y. Miyamoto, J. Light. Technol. **34**, 582 (2016).
4. N. Riesen, J. D. Love, and J. W. Arkwright, IEEE Photonics Technol. Lett. **24**, 344 (2012).
5. G. Milione, E. Ip, M.-J. Li, J. Stone, G. Peng, and T. Wang, Opt. Lett. **41**, 2755 (2016).
6. P. Sillard, M. Astruc, D. Boivin, H. Maerten, and L. Provost, in European Conference and Exposition on Optical Communications (OSA, 2011), p. Tu.5.LeCervin.7.
7. B. Huang, N. K. Fontaine, R. Ryf, B. Guan, S. G. Leon-Saval, R. Shubochkin, Y. Sun, R. Lingle, and G. Li, Opt. Express **23**, 224 (2015).
8. G. Labroille, B. Denolle, P. Jian, P. Genevaux, N. Treps, and J.-F. Morizur, Opt. Express **22**, 15599 (2014).
9. N. Riesen, S. Gross, J. D. Love, and M. J. Withford, Opt. Express **22**, 29855 (2014).
10. J. Dong, K. S. Chiang, and W. Jin, Opt. Lett. **40**, 3125 (2015).
11. J. Dong, K. S. Chiang, and W. Jin, J. Light. Technol. **33**, 4580 (2015).
12. N. Hanzawa, K. Saitoh, T. Sakamoto, T. Matsui, K. Tsujikawa, T. Fujisawa, Y. Ishizaka, and F. Yamamoto, in European Conference on Optical Communication (2015), p. 1.
13. K. J. Park, K. Y. Song, Y. K. Kim, J. H. Lee, and B. Y. Kim, Opt. Express **24**, 3543 (2016).
14. S. Gross, N. Riesen, J. D. Love, and M. J. Withford, Laser Photonics Rev. **8**, L81 (2014).
15. T. Watanabe and Y. Kokubun, IEEE Photonics J. **7**, 1 (2015).
16. J. B. Driscoll, R. R. Grote, B. Souhan, J. I. Dadap, M. Lu, and R. M. Osgood, Opt. Lett. **38**, 1854 (2013).
17. W. Chen, P. Wang, T. Yang, G. Wang, T. Dai, Y. Zhang, L. Zhou, X. Jiang, and J. Yang, Opt. Lett. **41**, 2851 (2016).
18. A. M. Velazquez-Benitez, J. C. Alvarado, G. Lopez-Galmiche, J. E. Antonio-Lopez, J. Hernández-Cordero, J. Sanchez-Mondragon, P. Sillard, C. M. Okonkwo, and R. Amezcua-Correa, Opt. Lett. **40**, 1663 (2015).
19. J. Dong and K. S. Chiang, IEEE Photonics Technol. Lett. **27**, 1006 (2015).

Full references

1. D. J. Richardson, J. M. Fini, and L. E. Nelson, "Space-division multiplexing in optical fibres," Nat. Photonics **7**(5), 354–362 (2013).
2. G. Li, N. Bai, N. Zhao, and C. Xia, "Space-division multiplexing: the next frontier in optical communication," Adv. Opt. Photonics **6**(4), 413–487 (2014).
3. T. Mizuno, H. Takara, A. Sano, and Y. Miyamoto, "Dense space-division multiplexed transmission systems using multi-core and multi-mode fiber," J. Light. Technol. **34**(2), 582–592 (2016).
4. N. Riesen, J. D. Love, and J. W. Arkwright, "Few-mode elliptical-core fiber data transmission," IEEE Photonics Technol. Lett. **24**(5), 344–346 (2012).
5. G. Milione, E. Ip, M.-J. Li, J. Stone, G. Peng, and T. Wang, "Mode crosstalk matrix measurement of a 1 km elliptical core few-mode optical fiber," Opt. Lett. **41**(12), 2755–2758 (2016).
6. P. Sillard, M. Astruc, D. Boivin, H. Maerten, and L. Provost, "Few-mode fiber for uncoupled mode-division multiplexing transmissions," in *European Conference and Exposition on Optical Communications* (OSA, 2011), p. Tu.5.LeCervin.7.
7. B. Huang, N. K. Fontaine, R. Ryf, B. Guan, S. G. Leon-Saval, R. Shubochkin, Y. Sun, R. Lingle, and G. Li, "All-fiber mode-group-selective photonic lantern using graded-index multimode fibers," Opt. Express **23**(1), 224–234 (2015).
8. G. Labroille, B. Denolle, P. Jian, P. Genevaux, N. Treps, and J.-F. Morizur, "Efficient and mode selective spatial mode multiplexer based on multi-plane light conversion," Opt. Express **22**(13), 15599–15607 (2014).
9. N. Riesen, S. Gross, J. D. Love, and M. J. Withford, "Femtosecond direct-written integrated mode couplers," Opt. Express **22**(24), 29855–29861 (2014).
10. J. Dong, K. S. Chiang, and W. Jin, "Mode multiplexer based on integrated horizontal and vertical polymer waveguide couplers," Opt. Lett. **40**(13), 3125–3128 (2015).
11. J. Dong, K. S. Chiang, and W. Jin, "Compact three-dimensional polymer waveguide mode multiplexer," J. Light. Technol. **33**(22), 4580–4588 (2015).
12. N. Hanzawa, K. Saitoh, T. Sakamoto, T. Matsui, K. Tsujikawa, T. Fujisawa, Y. Ishizaka, and F. Yamamoto, "Demonstration of PLC-based six-mode multiplexer for mode division multiplexing transmission," in *European Conference on Optical Communication* (2015), pp. 1–3.
13. K. J. Park, K. Y. Song, Y. K. Kim, J. H. Lee, and B. Y. Kim, "Broadband mode division multiplexer using all-fiber mode selective couplers," Opt. Express **24**(4), 3543–3549 (2016).
14. S. Gross, N. Riesen, J. D. Love, and M. J. Withford, "Three-dimensional ultra-broadband integrated tapered mode multiplexers," Laser Photonics Rev. **8**(5), L81–L85 (2014).
15. T. Watanabe and Y. Kokubun, "Demonstration of mode-evolutional multiplexer for few-mode fibers using stacked polymer waveguide," IEEE Photonics J. **7**(6), 1–11 (2015).
16. J. B. Driscoll, R. R. Grote, B. Souhan, J. I. Dadap, M. Lu, and R. M. Osgood, "Asymmetric Y junctions in silicon waveguides for on-chip mode-division multiplexing," Opt. Lett. **38**(11), 1854–1856 (2013).
17. W. Chen, P. Wang, T. Yang, G. Wang, T. Dai, Y. Zhang, L. Zhou, X. Jiang, and J. Yang, "Silicon three-mode (de)multiplexer based on cascaded asymmetric Y junctions," Opt. Lett. **41**(12), 2851–2854 (2016).
18. A. M. Velazquez-Benitez, J. C. Alvarado, G. Lopez-Galmiche, J. E. Antonio-Lopez, J. Hernández-Cordero, J. Sanchez-Mondragon, P. Sillard, C. M. Okonkwo, and R. Amezcua-Correa, "Six mode selective fiber optic spatial multiplexer," Opt. Lett. **40**(8), 1663–1666 (2015).
19. J. Dong and K. S. Chiang, "Temperature-insensitive mode converters with CO_2-laser written long-period fiber gratings," IEEE Photonics Technol. Lett. **27**(9), 1006–1009 (2015).